OPEN ACCESS

TRANSLATIONAL SCIENCE

Expression of HIF1α in intestinal epithelium restricts arthritis inflammation by inhibiting RIPK3-induced cell death machinery

Pang Lyu,[1,2] Jinming Wen,[1,2] Wenshuo Zhang,[1,2] Ning Liu,[1,2] Iris Stolzer,[2,3] Andreas Gießl,[4] Yewei Jia,[1,2] Daniele Mauro ,[5] Fulin Zhang,[1,2] Francesco Ciccia ,[5] Didier Soulat,[6] Claudia Günther,[2,3] Georg Schett ,[1,2] Aline Bozec [1,2]

Handling editor Josef S Smolen

► Additional supplemental material is published online only. To view, please visit the journal online (https://doi.org/10.1136/ard-2023-224491).

For numbered affiliations see end of article.

Correspondence to
Professor Aline Bozec, Department of Internal Medicine 3 Rheumatology and Immunology, FAU, Erlangen, Bayern, Germany; aline.bozec@uk-erlangen.de

PL and JW contributed equally.

Received 6 June 2023
Accepted 28 February 2024
Published Online First 19 March 2024

ABSTRACT

Objectives To investigate the mechanism by which intestinal epithelial cell (IEC) death induces arthritis.

Methods IEC death was assessed by staining for necroptosis and apoptosis markers and fluorescence in situ hybridisation at different time points during collagen-induced arthritis (CIA). During the development of CIA, messenger RNA (mRNA) sequencing was performed, followed by Gene Ontology enrichment analysis of differentially expressed genes. Mice deficient for hypoxia-inducible factor 1α (*Hif1a*) in IECs (*Hif1a*$^{\Delta IEC}$) were generated and induced for arthritis. mRNA sequencing, chromatin immunoprecipitated (ChIP) DNA sequencing and ChIP-qualitative PCR were performed on IECs from *Hif1a*$^{\Delta IEC}$ mice and littermate controls. Effects of HIF1α stabilisation by inhibition of prolyl hydroxylase domain-containing enzymes and treatment with the inhibitor of receptor-interacting protein kinase-3 (RIPK3) were tested in intestinal organoids and in CIA.

Results IEC underwent apoptotic and necroptotic cell death at the onset of arthritis, leading to impaired gut barrier function. HIF1α was identified as one of the most upregulated genes in IECs during the onset of arthritis. Deletion of *Hif1a* in IEC enhanced IEC necroptosis, triggered intestinal inflammation and exacerbated arthritis. HIF1α was found to be a key transcriptional repressor for the necroptosis-inducing factor RIPK3. Enhanced RIPK3 expression, indicating necroptosis, was also found in the intestinal epithelium of patients with new-onset rheumatoid arthritis. Therapeutic stabilisation of HIF1α as well as small-molecule-based RIPK3 inhibition rescued intestinal necroptosis in vitro and in vivo and suppressed the development of arthritis.

Conclusion Our results identify IEC necroptosis as a critical link between the gut and the development of arthritis.

WHAT IS KNOWN ON THIS TOPIC

⇒ The gut and the joints form a functional unit. Several studies have shown that intestinal inflammation can lead to the aggravation of arthritis. The pathways that link intestinal pathology to arthritis are incompletely understood.

WHAT THIS STUDY ADDS

⇒ This study shows that the death of intestinal epithelial cells via necroptosis is an important factor that promotes the onset of arthritis. Inhibition of intestinal epithelial cell necroptosis by pharmacologically stabilising hypoxia-inducible factor 1α or by blocking receptor-interacting protein kinase-3 inhibits the development of arthritis

HOW THIS STUDY MIGHT AFFECT RESEARCH, PRACTICE AND POLICY

⇒ This study opens up new avenues for inhibiting arthritis by improving gut barrier function.

INTRODUCTION

The intestinal barrier coordinates nutrient absorption, bacterial symbiosis and the immune system.[1] The integrity of the intestinal barrier is considered to influence the development of inflammatory arthritis, suggesting a link between intestinal pathology and arthritis.[2] Intestinal pathology characterised by abnormal immune cell infiltration and dysbiosis has been observed in the preclinical phase of rheumatoid arthritis (RA).[3 4] The monolayer of intestinal epithelial cells (IECs), connected by tight junctions and encapsulated within the mucus, constitutes the crucial part of this mechanical barrier. If this barrier is destabilised ('leaky gut'), autoimmunity and systemic inflammation can arise.[5] In accordance, the maintenance of the intestinal barrier integrity, for example, by targeting tight junction proteins, alleviates inflammatory arthritis.[6 7] However, the role of IEC survival in the development of inflammatory arthritis is currently unknown.

Aberrant and excessive IEC death has been reported as a sign of progression in chronic inflammatory bowel disease and necrotising enterocolitis.[8 9] Necroptosis of the IEC disconnects tight junctions and lowers intestinal barrier integrity, thereby shifting it to a proinflammatory milieu both in experimental and human colitis.[10–12] This phenotype is strongly linked to microbial dysbiosis and chronic intestinal inflammation, characterised by mucosal and systemic Th17 responses.[10–12] To date, the role of IEC death in the development of arthritis is, however, unclear.

Intestinal inflammation consumes large amounts of oxygen, rendering the inflamed tissue

Check for updates

To cite: Lyu P, Wen J, Zhang W, *et al*. *Ann Rheum Dis* 2024;**83**:984–997.

hypoxic.[13 14] Hypoxia activates a highly conserved family of transcription factors, among which hypoxia-inducible factor (HIF) 1α and HIF2α are controlling these metabolic processes.[15] By transcriptionally enhancing claudin-15 expression, which impairs tight junctions in the intestinal barrier, HIF2α allows the opening of the intercellular tight junction and promotes arthritis.[7] Conversely, in the context of chronic intestinal inflammation, HIF1α increases barrier function, elicits protective innate immune responses and activates antimicrobial responses.[16–18] Therefore, HIF1α expression and stabilisation in IECs might also influence arthritis. Here, we observed that HIF1α had a critical role in IEC survival as it inhibited necroptosis of IEC. This effect was mediated by the control of receptor-interacting protein kinase-3 (RIPK3), a central mediator for necroptosis. In the absence of HIF1α, IEC death shifted from physiological apoptosis to pathological necroptosis and triggered mucosal barrier dysfunction and arthritis. Stabilisation of HIF1α by roxadustat or inhibition of RIPK3 by GSK'872 maintained intestinal barrier function and ameliorated the development of arthritis. These data suggest that RIPK3-mediated epithelial cell necroptosis is a critical factor in linking gut pathology to the development of arthritis.

METHODS

Human tissue

Sample information was described previously.[7] Briefly, ileal biopsies from healthy individuals and patients with new-onset RA were used for the present study. Paraffin-embedded sections were subjected to immunofluorescence staining for HIF1α (Cayman). Nuclei were visualised by 4′,6-diamidino-2-phenylindole (DAPI) staining (Life Technologies). Paraffin-embedded sections were subjected to immunohistochemistry staining for RIPK1 (CellSignal), RIPK3 (CellSignal) and MLKL (Biorbyt). Confocal microscopy was used to screen the slides. HIF1α-positive cells were counted from three random high-power microscopic fields (×400 magnification). Immunohistochemistry staining of RIPK1, RIPK3 and MLKL was quantitatively scored, ranging from 0 (no staining) to 5 fully stained from three random high-power microscopic fields (×400 magnification).

Mice

C57BL/6 wild-type (WT) mice (6–8 weeks old) and DBA1/J (8 weeks old) were purchased from Janvier Laboratories. Epithelial-specific HIF1α-deficient mice ($Hif1a^{\Delta IEC}$) were generated by crossing $Hif1a^{flox/flox}$ mice with Villin-cre mice. $Hif1a^{flox/flox}$ mice and Villin-cre mice were previously reported.[19 20] $Ripk3^{-/-}$, $Mlkl^{-/-}$, $Ripk3^{-/-}Mlkl^{-/-}$ mice were previously described and acquired from Professor Claudia Günther's laboratory (FAU Germany).[21 22] The genetically modified mice were maintained on a C57BL/6 background. $Hif1a^{flox/flox}$ cre-negative or $Hif1a^{+/+}$ cre-positive littermates were considered as controls. The experiments were approved by the local ethics committee of the Regierung von Mittelfranken.

Collagen-induced arthritis (CIA) model

Mice were injected twice (days 1 and 21) with 100 μL of 0.25 mg chicken type II collagen emulsified in complete Freunds' adjuvant (Sigma) at the base of the tail. The clinical score of each paw was assessed every other day by the same person. Scores were recorded on a scale of 0–4, as previously described.[7]

Treatments

Mice were orally given a vehicle or prolyl-hydroxylase domain (PHD) inhibitor (FG-4592, Medchemexpress, 20 mg/kg) or RIPK3 inhibitor, GSK'872 (Medchemexpress, 7.5 mg/kg) every other day from day 6 post-first immunisation (pfi) until day 36 pfi.

Flow cytometry

Single-cell suspensions were harvested from Peyer's patches, mesenteric lymph nodes and spleen. Following Fc-blocking (CD16/CD32), cells were stained with antibodies (Supplementary table 1). The expression of cell surface molecules was analysed by a Cytoflex (Beckman Coulter) flow cytometer. LIVE/DEAD Fixable Orange (602) Viability Kit (L34983, Invitrogen) was used to exclude dead populations before analysis. For Th1 and Th17 cell analysis, phorbol-12-myristate-13-acetate (20 ng/mL), ionomycin (1 μg/mL) and monensin (L+PIM) were added to the culture medium 5 hours before fixation. Foxp3/Transcription Factor Staining Buffer Set (00/5523/00, eBioscience) was used for membrane permeabilisation. The analyses were performed with the CytExpert V.2.4 software.

IEC isolation

Small intestines were dissected, washed with ice-cold phosphate-buffered saline (PBS) containing 0.154 M sodium chloride (NaCl) and 1 mM dithiothreitol (DTT) and cut into 0.5-cm fragments, which were incubated with 1.5 mM EDTA and 0.5 mM DTT for 30 min. After incubation, the intestinal fragments were washed in the same buffer and vortexed to detach the intestinal epithelium. Acquired supernatants were filtered through a 70-μm cell strainer twice to isolate single cells.

RNA isolation and quantitative real-time (qRT) PCR analysis

The total RNA of a cell or tissue was extracted with Trizol (Invitrogen), and complementary DNA (cDNA) was synthesised with a HighCapacity cDNA Reverse Transcription Kit (4368814, Thermo Scientific). qRT-PCR was performed using SYBR Green I-dTTP (Eurogentec). Primers were listed in online supplementary table 2. The relative expression of a target gene was calculated according to the ΔΔCt method.

Organoids culture

Small intestine organoids were cultured as previously described.[23] Tissue was dissected and washed, and intestinal villi were scraped out of the epithelium. After incubation in dissociation buffer (PBS with 2 mM EDTA), intestinal crypts were isolated and seeded in matrigel (BD Bioscience). Culture medium (advanced Dulbecco's modified Eagle medium (DMEM)/F12 (Invitrogen), 10 mM (4-(2-hydroxyethyl)-1-piperazineethanesulfonic acid (HEPES), 2 mM GlutaMax (Invitrogen), 100 U/mL penicillin–streptomycin (Gibco), 50 ng/mL murine epidermal growth factor (Immunotools), 1 mg/mL recombinant human R-spondin (R&D Systems), 1 mg/mL B27 (Invitrogen), 1 mM N-acetylcysteine (Sigma-Aldrich) and 50 ng/mL recombinant murine Noggin (Peprotech) were changed every 3 days.

RNA-seq analysis

cDNA library and RNA-seq were conducted by NovogeneEurope (Cambridge Science Park, UK) on the Illumina HiSeq 2500 platform. The raw data were first quality-controlled (fastqc v0.11.8) and then the adapter and low-quality reads were removed (fastqc v0.11.8). The cleaned data were mapped to the reference genome GRCm38 (star v2.6.1c). Then transcripts

were assembled to obtain count numbers for each gene (samtools v1.8, subread v1.6.1). Count data were normalised and subjected to downstream analysis and visualisation in RStudio (R V.4.1.1.) software. The RNA-seq data used in this paper have been uploaded to the GEO databases (GSE175907, GSE176266 and GSE225597).

Micro-CT (µCT)

Mice's hind paws were fixed overnight in 4% paraformaldehyde and measured by the cone-beam system (SCANCO Medical AG, Bruettisellen, Switzerland) at 55 Kv, 177 μA and 200 ms integration time. The isotropic size was 8.6 μm.

Histology

Paws were fixed overnight in 4% paraformaldehyde, decalcified in 14% EDTA for 2 weeks and embedded in paraffin. Sections of 5-μm thickness were generated from the paraffin tissue blocks, and then H&E and tartrate-resistant acid phosphatase (TRAP) staining were performed. Intestines were cut into 5-μm sections. After 4% paraformaldehyde fixation and paraffin embedment, H&E or periodic acid Schiff (PAS) stains were performed. Intestinal histological scores were assessed on H&E slides following published criteria.[24]

Fluorescence staining

Sections were deparaffinised and epitopes were retrieved by the heat-induced method at 95°C for 10 min in sodium citrate buffer (10 mM sodium citrate, pH 6.0). Sections were blocked with 5% bovine serum albumin and 2% horse serum at room temperature for 1 hour. Sections were incubated with the primary antibodies listed in supplementary table 1 . Immunofluorescence was realised following published protocols.[25] BZ-X700-All-in-One Fluorescence Microscope (Keyence) or Carl Zeiss LSM 700 Laser Scan Confocal Microscope (confocal fluorescence microscopy) were used for capturing images.

Fluorescence in situ hybridisation (FISH)

Ileal sections were deparaffined, rehydrated and incubated in hybridisation buffer (20 mM Tris–hydrochloric acid, 0.9 M NaCl and 0.1% sodium dodecyl sulphate) for 10 min at 50°C. Then, sections were incubated with 100 nM 16S rRNA-targeted bacterial probes (5′−3′: GCTGCCTCCCGTAGGAGT, fluorescein isothiocyanate (FITC)-conjugated; Sigma) in the hybridisation buffer for 4 hours at 50°C and mounted with DAPI. A keyence microscope was used for imaging acquisition. Bacterial probe signal intensity was quantified by measuring the positive area for FITC fluorescence.

Chromatin immunoprecipitation sequencing and qRT-PCR (ChIP-Seq and ChIP-qPCR)

IECs were isolated from *Hif1a*$^{\Delta IEC}$ mice and littermate control mice at day 36 pfi. HIF1α ChIP experiments were performed with the ChIP-IT Express kit (53040, Active Motif) using IgG as a control. The enriched DNA was sequenced in NovogeneEurope. ChIP-Seq raw data were processed on the EU server of the Galaxy Community Hub. Quality control was performed using FastQC; short reads were mapped using Bowtie2, and peak calling was performed using MACS2. The peak annotation was performed using the R package ChIPseeker. Genome distribution and peak visualisation were processed by the IGV V.2.13.1 software. Primers targeting *Ripk1, Ripk3* and *Mlkl* promoter hormone response elements (HREs) were listed (online table 2). HIF1α or HIF2α were predicted to bind on the same core element (A/GCGTG) in the JASPAR database, and ChIP primers were designed by Primer-BLAST. The ChIP-Seq data used in this paper have been uploaded to the GEO database (GSE225594).

Cell line culture and transfection

MC38 cells (C57BL6 murine colon adenocarcinoma cell line) were cultured in DMEM, supplemented with 10% (v/v) fetal bovine serum (GIBCO, Invitrogen) and 1% penicillin/streptomycin at 37°C under a 5% carbon dioxide humidified atmosphere. A lipofectamine 3000 transfection kit (Invitrogen, L3000001) was used for transfections according to the manufacturer's recommendations. HIF1α short hairpin RNA (shRNA) plasmid (pLV(shRNA)-U6>mHif1a, Plasmid#VB900122-2421ngn, Biozol/Vectorbuilder) was used for HIF1α knockdown. To assess knockdown efficiency, transfected cells were checked by western blot after 1% hypoxic treatment for 8 hours.

Dual luciferase reporter assay

Ripk1, Ripk3 and *Mlkl* promoter HREs (online supplementary table 2) were amplified by PCR from genomic DNA extracted from splenocytes in C57BL/6 WT mice and cloned using HINDIII and NheI (New England Biolabs) into the pGL4.23 firefly reporter vector, respectively (Promega). The recombinant vectors were sequenced in Microsynth Seqlab (Göttingen, Germany) to validate the presence of inserted HREs. MC38 cells were co-transfected with luciferase reporter plasmids, HIF1α or HIF2α TM plasmids (Addgene) and Renilla plasmids (Addgene) using the Lipofectamine 3000 kit (Invitrogen). After 48 hours of culture, cells were lysed, and luciferase activity was measured and normalised to Renilla activity.

ELISA

Interleukin (IL)-17A and interferon-gamma (IFN-γ) levels were measured by commercial ELISA (88-7371-88 and 88-7314-88 Invitrogen, respectively).

Statistical analysis

Data are expressed as mean±SD. The data distribution was tested by the Shapiro-Wilk or Kolmogorov-Smirnov tests. A two-tailed unpaired Student's t-test or Mann-Whitney U test was used for a single comparison. One-way or two-way analysis of variance (ANOVA) followed by Tukey's or Bonferroni's test, multiple t-tests and the Kruskal-Wallis H test followed by Dunn's test were used for multiple comparisons. For multiple comparisons, non-normal distributed data were transformed by a square root or logarithm. Kaplan-Meier analysis with a log-rank test and χ^2 test were used for survival curve or incidence comparisons. All experiments were repeated at least two times. P values of 0.05 were considered statistically significant and are shown as *p<0.05, **p<0.01, ***p<0.001 and ****p<0.0001. Graph generation and statistical analyses were performed using the Prism V.9 software (GraphPad, La Jolla, CA, USA).

RESULTS

IEC death at the onset of experimental arthritis

To determine IECs' integrity during the course of CIA, we delineated the translocation of intestinal bacteria as macroscopic evidence of barrier dysfunction. Using a bacterial-specific probe for FISH, bacterial translocation could be detected in the ileum shortly before (day 29 pfi) and at the onset of CIA (day 36 pfi) (figure 1A and C). The death of ileum IECs was detected by terminal deoxynucleotidyl transferase dUTP nick end labelling (TUNEL) staining (figure 1B and D) and electron microscopy

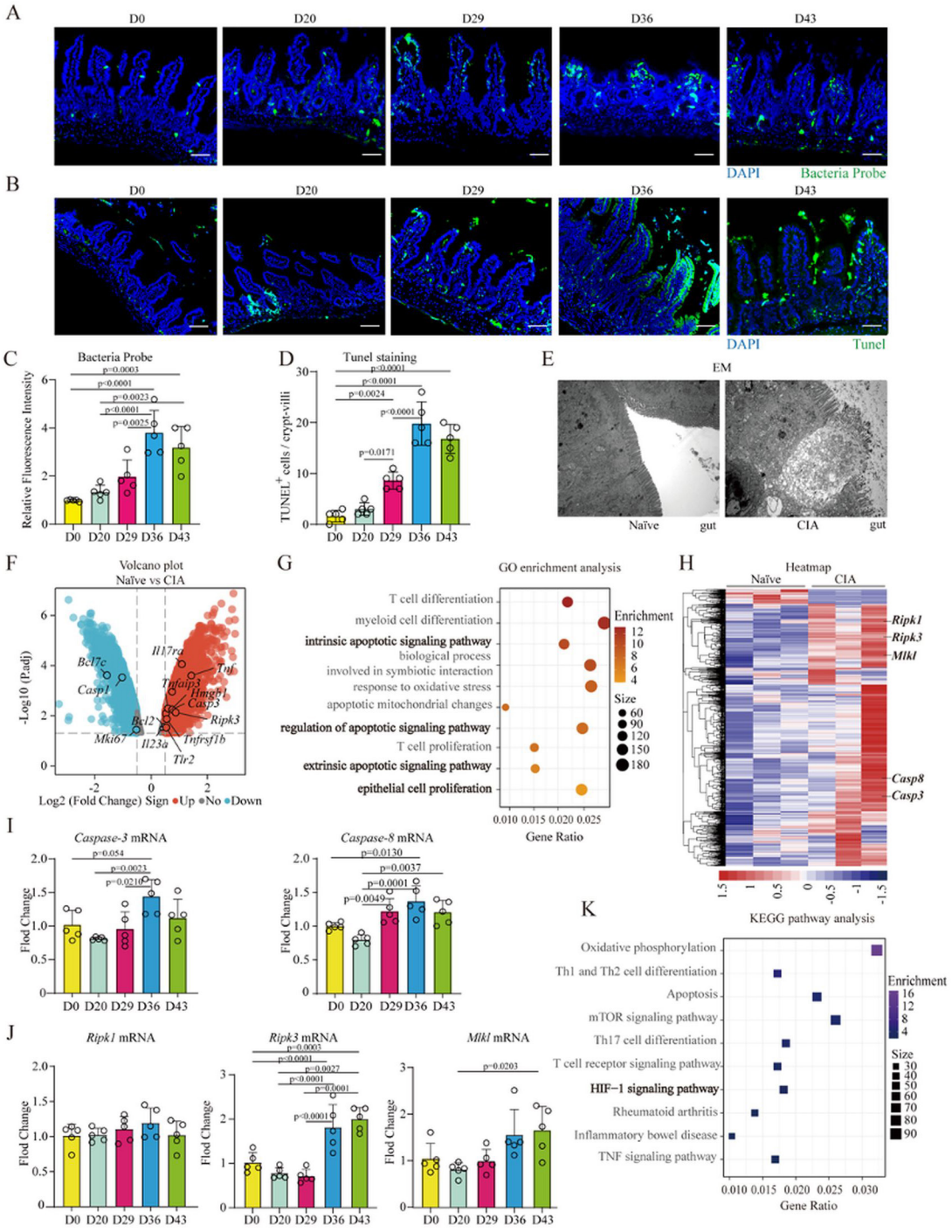

Figure 1 IEC death at the onset of experimental arthritis. Representative pictures and quantification of fluorescence in situ hybridisation using the bacteria-specific probe EUB 338-fluorescein isothiocyanate (green) (A and C) and TUNEL staining for cell death (green) (B and D) on ileal sections in DBA/1 mice subjected to CIA at indicated days pfi (n=5); nuclei visualisation by DAPI (blue); scale bar 50 µm. (E) EM showing the intestinal epithelial barrier in the ileum of mice induced for CIA or non-induced C57BL/6 mice at day 36 pfi; scale bar 1 µm. (F) Volcano plot of RNA bulk sequencing showing the DEGs in IECs from mice induced for CIA or non-induced C57BL/6 mice at day 36 pfi (n=3). (G) GO enrichment analysis of the DEGs. Enriched pathways are presented in a dot plot. (H) Heatmap of the DEGs. (I and J) Quantitative real-time PCR analysis of *Caspase-3*, *Caspase-8*, *Ripk1*, *Ripk3* and *Mlkl* mRNA expression in IECs from the ileum of DBA/1 mice induced for CIA (n=5). (K) KEGG pathway enrichment analysis of the DEGs; enriched pathways are presented in a dot plot; symbols represent individual C57BL/6 mice; data are shown as mean±SD. Statistical significance was determined by a one-way analysis of variance (C, D, I and J) followed by Tukey's test for multiple comparisons. CIA, collagen-induced arthritis; DAPI, 4′,6-diamidino-2-phenylindole; DEGs, differentially expressed genes; EM, electron microscopy; GO, Gene Ontology; HIF, hypoxia-inducible factor; IEC, intestinal epithelial cell; KEGG, Kyoto Encyclopedia of Genes and Genomes; pfi, post-first immunisation; TUNEL, terminal deoxynucleotidyl transferase dUTP nick end labelling.

(figure 1E). However, no significant increase in bacterial translocation or cell death was shown in the colon (online supplemental figure 1A–D). To elucidate the cell death machinery at play, IECs from the small intestine were isolated at the onset of arthritis (day 36 pfi) and analysed by bulk-RNA sequencing. The volcano plot (figure 1F) and Gene Ontology (GO) enrichment analyses (figure 1G) indicated a significant alteration of the apoptotic pathway at the onset of arthritis. Among the differentially expressed genes, *Caspase-3*, *Caspase-8*, *Ripk1*, *Ripk3* and the *Mlkl* gene were significantly increased in IECs from arthritic mice compared with non-arthritic controls (figure 1H). These results were confirmed by qRT-PCR analysis (figure 1I) and immune fluorescence, indicating upregulation of cleaved caspase-3 and caspase-8 (online supplemental figure 2A–C) as well as key proteins involved in necroptosis, such as p-RIPK1, p-RIPK3 and p-MLKL in IEC at the onset of arthritis (day 36 pfi; figure 1, online supplemental figure 2D–G), suggesting that substantial death of IECs occurs at the onset of arthritis.

HIF1α expression in gut epithelial cells controls the development of arthritis

To identify a putative molecular correlation between the increased necroptosis markers and arthritis, we further analysed the Kyoto Encyclopedia of Genes and Genomes (KEGG) pathway enrichment results obtained from IEC bulk-RNA sequencing. The T cell differentiation pathways and the HIF1α pathway were significantly enhanced in IEC at the onset of arthritis (figure 1K). Immunofluorescence staining of HIF1α in ileum biopsies from patients diagnosed with new-onset RA showed increased HIF1α expression in IECs compared with healthy controls (figure 2A and B). Similarly, *Hif1α* mRNA expression was increased at the onset of CIA (day 36 pfi), while protein expression was elevated even earlier in the murine model (day 20 pfi; figure 2C–E). To dissect the function of HIF1α in the intestinal epithelium, we generated IEC-specific HIF1α knockout mice ($Hif1a^{\Delta IEC}$). Selective expression of *Villin* gene expression in IECs was reported using *Villin-cre;Rosa26* tdTomato naive mice (online supplemental figure 3A). Subsequently, 90% HIF1α knockout efficiency in IECs was confirmed by qRT-PCR and western blot in IECs from $Hif1a^{\Delta IEC}$ mice (online supplemental figure 3B–E). Interestingly, $Hif1a^{\Delta IEC}$ mice subjected to CIA showed more severe (figure 2F) and earlier onset (figure 2G) arthritis than littermate controls. $Hif1a^{\Delta IEC}$ mice presented increased paw thickness (figure 2H), bone erosion, synovial inflammation and osteoclast numbers (figure 2I and J). IFN-γ and IL-17A serum levels were increased in $Hif1a^{\Delta IEC}$ mice (figure 2K) as well as Th1 and Th17 cell numbers in the Payer's patches (PPs; figure 2L), mesenteric lymph nodes (MLN; figure 2M) and the spleen (figure 2N). IgA+B220 cells were also increased in PP and MLN of arthritic $Hif1a^{\Delta IEC}$ mice (online supplemental figure 3F). Together, these results point to a protective role of HIF1α expression in IECs against the development of arthritis.

Induction of HIF1α alleviates arthritis and inhibits intestinal epithelial cell death

To further investigate the role of HIF1α in arthritis, we treated mice with roxadustat, which stabilises HIF expression by inhibiting PHD protein. Roxadustat treatment (oral gavage every other day) reduced the clinical score (figure 3A) and the incidence of arthritis (figure 3B) compared with vehicle treatment. Paw swelling, synovial inflammation, bone erosion and osteoclast numbers tend to reduce (figure 3C and D, online supplemental figure 4A–C). Intestinal inflammation was suppressed in roxadustat-treated CIA mice, as shown by reduced inflammatory areas and intestinal bacterial translocation (figure 3, online supplemental figure 4D–F). Except in the spleen, flow cytometry analysis of lymphocytes from PPs and MLN showed decreased Th1 and Th17 cell infiltration in roxadustat-treated CIA mice (figure 3), which were associated with lower serum IFN-γ and IL-17A levels (figure 3I). IgA+B220 cells were decreased in the PPs but not in the MLN or spleen (online supplemental figure 4G and H), while Treg cells were increased in the PPs and MLN, indicating the induction of an immune regulatory environment in the gut of roxadustat-treated CIA mice (online supplemental figure 4I and J).

Next, we tested whether roxadustat alters HIF1α and HIF2α expression in IECs. While there was no significant effect on HIF2α, HIF1α protein level was significantly increased by the treatment (figure 3J). TUNEL staining and electron microscopy scans confirmed that roxadustat protected IEC viability (figure 3K, online supplemental figure 4K). mRNA levels of *caspase-3*, *caspase-8*, *ripk3* and *mlkl*, but not *Ripk1*, were decreased in IECs from roxadustat-treated CIA mice (figure 3L and M). Protein levels of cleaved caspase-3, cleaved caspase-8, RIPK3, MLKL and RIPK1 were also decreased in the IECs of roxadustat-treated CIA mice (figure 3N). qRT-PCR analyses showed that *Caspase3*, *Caspase8*, *Ripk3*, *Mlkl*, *Hmgb1*, *Tnfrsf1a* and *Tnf* gene expression were decreased, while *Ripk1*, *Tnfrsf1b*, *Bax* and *Bcl-2* expression remained unchanged in organoid culture exposed to 1% oxygen after roxadustat treatment (online supplemental figure 4L). To investigate the involvement of HIF1α in cell death pathways, we stimulated WT and HIF1α-deficient organoids with tumor necrosis factor alpha (TNFα) and various Toll-like receptor agonists for 24 hours, with and without 20 μM roxadustat treatment. HIF1α-deficient organoids showed reduced viability after TNFα stimulation compared with WT organoids. Interestingly, roxadustat treatment only demonstrated a mitigating effect on TNFα-induced cell death in WT organoids (online supplemental figure 4M). Taking together, these data suggest that stabilisation of HIF1α in IECs supports their survival, maintains intestinal barrier function and ameliorates arthritis.

HIF1α expression preserves the gut epithelial cells from death

Of note, HIF1α deficiency did not affect gut integrity at a steady state, as characterised by the intestinal histology (online supplemental figure 5A–D) and the quantification of the Th1, Th17 and IgA+B220 populations in PPs, MLN and spleen (online supplemental figure 5E–H). However, in the case of CIA, histological sections of the ileum showed increased inflammation (figure 4, online supplemental figure 5I and J) and bacterial invasion (figure 4, online supplemental figure 5K) in $Hif1a^{\Delta IEC}$ compared with littermate control mice, while there was no significant change in mucus secretion (figure 4D, online supplemental figure 5L). TUNEL staining (figure 4, online supplemental figure 5M) and electron microscopy depicted increased epithelial cell death in $Hif1a^{\Delta IEC}$ CIA mice (figure 4F). We next isolated IECs from non-induced and CIA-induced WT and $Hif1a^{\Delta IEC}$ mice at the onset of arthritis (day 36 pfi) and subjected cells to RNA bulk sequencing. While IECs from non-induced WT and $Hif1a^{\Delta IEC}$ mice showed a very similar mRNA expression profile (figure 4G), 1837 genes were differentially expressed between WT and $Hif1a^{\Delta IEC}$ mice during CIA (figure 4H). GO and KEGG enrichment analyses suggested that HIF1α deletion affected genes controlling T cell activation and proliferation (figure 4I), confirming our previous fluorescence-activated

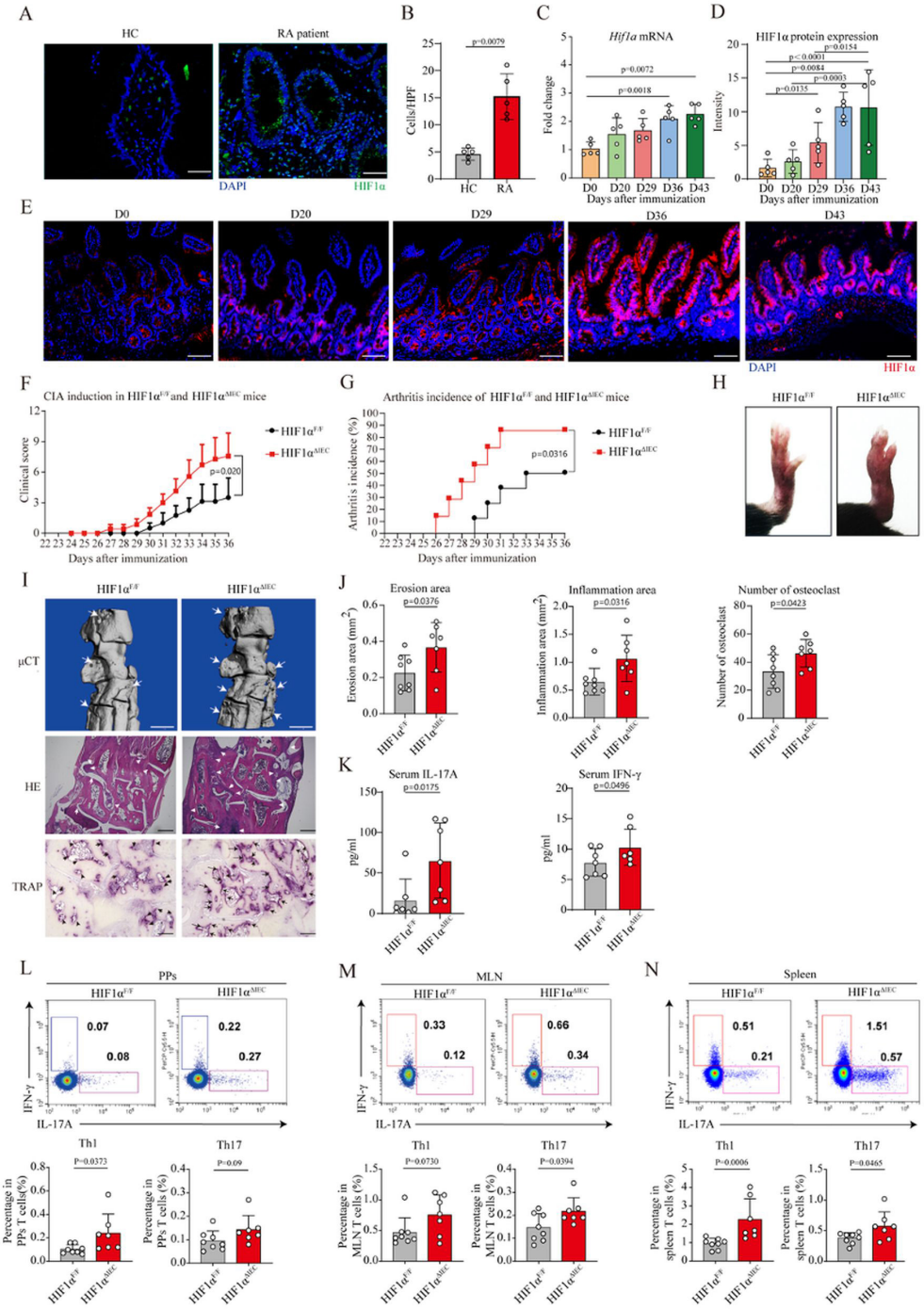

Figure 2 HIF1α expression in gut epithelial cells controls the development of arthritis. (A) IF and (B) quantification of HIF1α (green) and DAPI (blue) in the ileum of HC and patients with new-onset RA; scale bar 25 µm. (C) Quantitative real-time PCR analysis of *Hif1α* mRNA expression in ileal IECs from DBA/1 mice induced for CIA (n=5). (D) Quantifications and (E) representative pictures of HIF1α IF staining from ileal sections from DBA/1 mice induced for CIA; scale bar 50 µm . (F) Clinical score and (G) arthritis incidence in C57BL/6 mice with HIF1α-deletion in IECs (HIF1α$^{\Delta IEC}$) and their littermate control subjected to CIA (n=7 and 8, respectively). (H) Representative hind paw pictures from CIA-induced HIF1α$^{\Delta IEC}$ and littermate controls C57BL/6 mice at day 36 pfi. (I) Representative images of µCT scans, H&E staining and TRAP staining and (J) quantification of erosion area, inflammation area and osteoclast numbers in the hind paws of CIA-induced HIF1α$^{\Delta IEC}$ C57BL/6 mice and littermate controls at day 36 pfi (n=7 and 8, respectively). White arrowheads indicate inflammation (H&E) and bone erosion (TRAP, µCT); histology scale bar 50 µm; µCT scale bar 1 mm. (K) IL-17A and IFN-γ levels measured by ELISA in serum of CIA-induced HIF1α$^{\Delta IEC}$ C57BL/6 mice (n=7 and 6, respectively) and littermate controls at day 36 pfi (n=7). Representative fluorescence-activated cell sorting plots and quantification of Th17 cells (IL-17A+CD4+) and Th1 cells (IFN-γ+CD4+) in (L) PP, (M) mesenteric lymph nodes and (N) the spleen in CIA-induced HIF1α$^{\Delta IEC}$ C57BL/6 mice (n=7) and littermate controls (n=8) at day 36 pfi. Symbols represent individual mice. Data are shown as mean±SD. Statistical significance was determined by two-tailed unpaired (B, J–N) Student's t-test or Mann-Whitney U test, (C and D) one-way analysis of variance followed by (F) Tukey's test, Kaplan-Meier analysis with log-rank test and (G) χ^2 test. CIA, collagen-induced arthritis; DAPI, 4′,6-diamidino-2-phenylindole; HIF, hypoxia-inducible factor; IEC, intestinal epithelial cells; IF, immunofluorescence; HC, healthy individuals; IL, interleukin; IFN-γ, interferon-gamma; pfi, post-first immunisation; PP, Peyer's patches; µCT, micro-CT; RA, rheumatoid arthritis; TRAP, tartrate-resistant acid phosphatase.

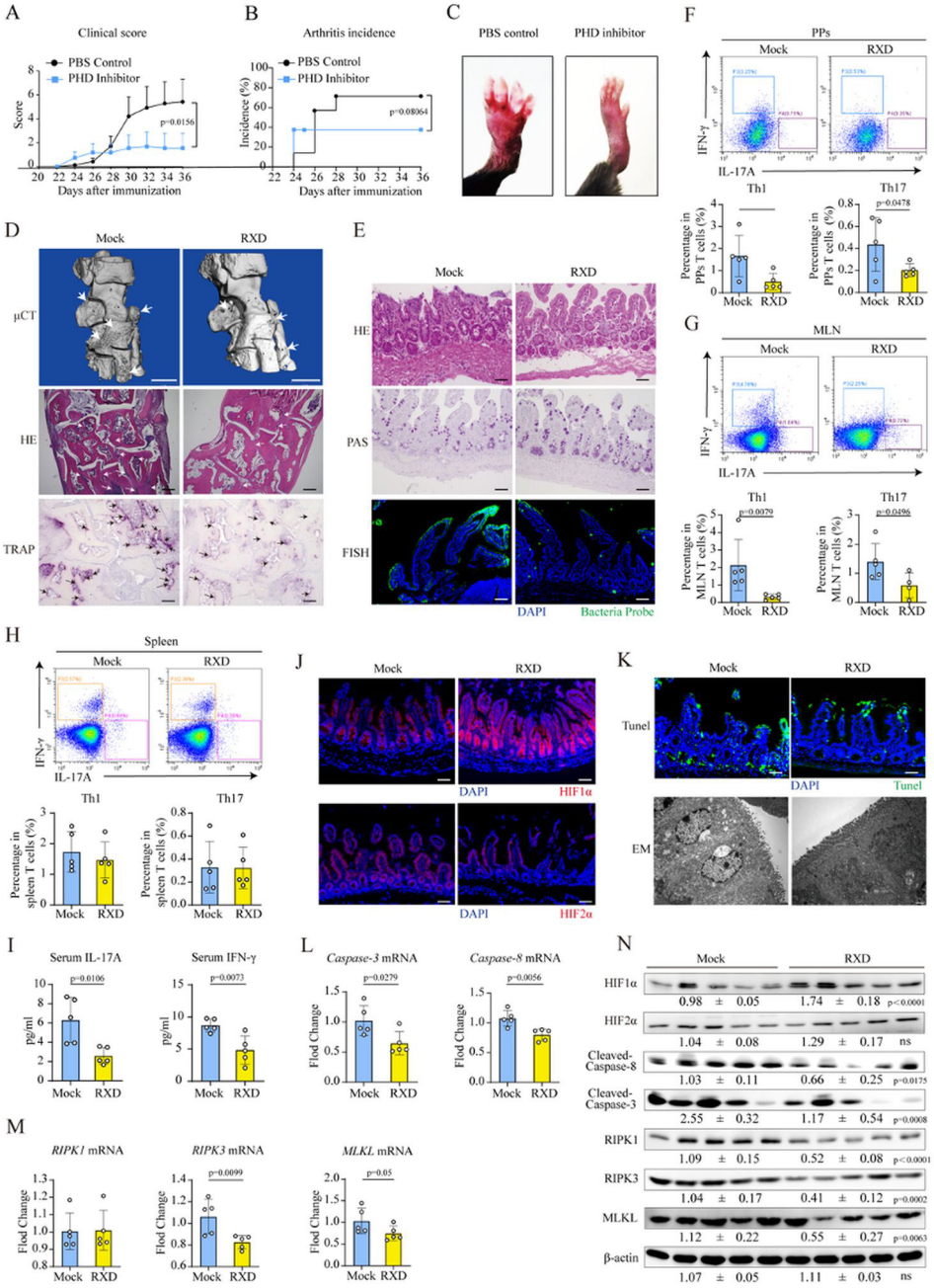

Figure 3 Pharmacological stabilisation of HIF1α inhibits arthritis and intestinal epithelial cell death. (A) Clinical score, (B) arthritis incidence and (C) representative paw picture from C57BL/6 mice induced for CIA and orally treated with PHD inhibitor RXD (n=12) or vehicle (n=13). (D) μCT scans, H&E staining and TRAP staining of the paws from C57BL/6 mice induced for CIA treated with RXD or vehicle at day 36 pfi. White arrows indicate inflammation (H&E) and bone erosion (TRAP, μCT); histology scale bar 50 μm. μCT scale bar 1 mm. (E) H&E, PAS and FISH staining of ileal sections of C57BL/6 mice induced for CIA and treated with RXD or vehicle at day 36 pfi (n=5); scale bar 50 μm. (F–H) Representative fluorescence-activated cell sorting plots and quantification of Th17 cells (IL-17A+CD4+) and Th1 cells (IFN-γ+CD4+) in the (F) PPs, (G) MLN and (H) spleen from C57BL/6 mice induced for CIA and treated with RXD or vehicle at day 36 pfi (n=5). (I) Serum IL-17A and IFN-γ levels in C57BL/6 mice induced for CIA and treated with RXD or vehicle at day 36 pfi (n=5). (J) Representative pictures of IF staining for HIF1α (red, upper panel), HIF2α (red, lower panel) and DAPI (blue); scale bar 50 μm. (K) Representative pictures of TUNEL staining (green) and nuclei visualisation by DAPI (blue) and EM pictures of ileal sections from C57BL/6 mice induced for CIA and treated with RXD or vehicle at day 36 pfi; TUNEL scale bar 50 μm. EM scale bar 1 μm. Quantitative-PCR analyses of (L) *Caspase-3*, *Caspase-8*, (M) *Ripk1*, *Ripk3* and *Mlkl* mRNA expression in IECs from C57BL/6 mice induced for CIA and treated with RXD or vehicle. (N) Western blot analysis of HIF1α, HIF2α cleaved caspases-3 and caspases-8, RIPK1, RIPK3 and MLKL of IECs from C57BL/6 mice induced for CIA and treated with RXD or vehicle at day 36 pfi. Actin was used as aPe loading control. Data are shown as mean±SD. Statistical significance was determined by Kaplan-Meier analysis with (A) log-rank test, (B) χ^2 test, two-tailed unpaired Student's t-test or Mann-Whitney U test. CIA, collagen-induced arthritis; DAPI, 4′,6-diamidino-2-phenylindole; EM, electron microscopy; FISH, fluorescence in situ hybridisation; HIF, hypoxia-inducible factor; IEC, intestinal epithelial cells; IF, immunofluorescence; HC, healthy individuals; IL, interleukin; IFN-γ, interferon-gamma; pfi, post-first immunisation; PAS, periodic acid Schiff; PP, Peyer's patches; PHD, prolyl-hydroxylase domain; μCT, micro-CT; RA, rheumatoid arthritis; MLN, mesenteric lymph nodes; RXD, roxadustat; TRAP, tartrate-resistant acid phosphatase; TUNEL, terminal deoxynucleotidyl transferase dUTP nick end labelling.

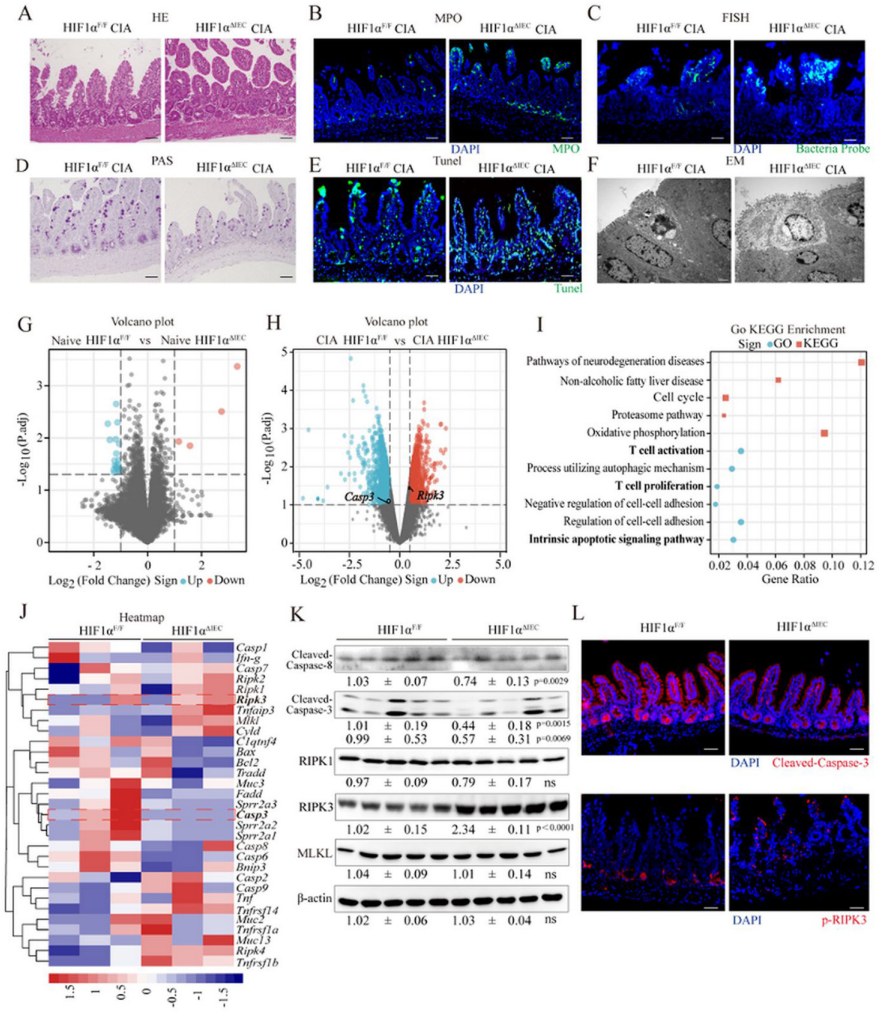

Figure 4 HIF1α expression protects from intestinal epithelial cell death. Representative images of (A) H&E staining, (B) MPO, (C) PAS, (D) FISH, (E) TUNEL staining and (F) EM from the ileum of HIF1α$^{\Delta IEC}$ mice and littermate controls with CIA at day 36 pfi; scale bar 50 µm. (G–H) Volcano plot of bulk RNA sequencing showing DEGs of ileal IECs from HIF1α$^{\Delta IEC}$ mice and littermate controls, which were induced or not induced for CIA (day 36 pfi; n=each 3). (I) Dot plot of GO and KEGG pathway enrichment analysis of the DEGs of ileal IECs from CIA-induced HIF1α$^{\Delta IEC}$ mice and littermate controls at day 36 pfi. (J) Heatmap of cell death-related DEGs in IECs from HIF1α$^{\Delta IEC}$ mice and littermate controls at day 36 pfi. (K) Western blot analysis of cleaved caspase-3 and caspase-8, RIPK1, RIPK3 and MLKL in IEC lysates from HIF1α$^{\Delta IEC}$ mice and littermate controls at day 36 pfi. (L) IF staining for cleaved caspase-3 (red, upper panel), p-RIPK3 (red,lower panel) and DAPI (blue) on ileal sections from HIF1α$^{\Delta IEC}$ mice and littermate controls at day 36 pfi. Data are shown as mean±SD. Statistical significance was determined by a two-tailed unpaired Student's t-test or Mann-Whitney U test (J). CIA, collagen-induced arthritis; DAPI, 4′,6-diamidino-2-phenylindole; DEGs, differentially expressed genes; EM, electron microscopy; FISH, fluorescence in situ hybridisation; GO, Gene Ontology; HIF, hypoxia-inducible factor; IEC, intestinal epithelial cells; IF, immunofluorescence; IL, interleukin; IFN-γ, interferon-gamma; KEGG, Kyoto Encyclopedia of Genes and Genomes; pfi, post-first immunisation; PAS, periodic acid Schiff; PP, Peyer's patches; PHD, prolyl-hydroxylase domain; µCT, micro-CT; MPO, myeloperoxidase; RA, rheumatoid arthritis; TRAP, tartrate-resistant acid phosphatase; TUNEL, terminal deoxynucleotidyl transferase dUTP nick end labelling.

cell sorting analysis (figure 2L–N). With respect to cell death, *Caspase-3* mRNA expression was downregulated, while the necroptosis gene *Ripk3* was upregulated in *Hif1a*$^{\Delta IEC}$ IEC from CIA-induced mice (figure 4J). Both changes were confirmed by western blot (figure 4K) and immunofluorescence of cleaved caspase-3 and phosphoryllated RIPK3 (p-RIPK3) (figure 4L). To further corroborate the interdependence between HIF1α and necroptosis markers, *Hif1α* was silenced by shRNA in the intestinal epithelial cell line MC38 under hypoxic conditions. Increased necroptotic markers (RIPK1, RIPK3 and MLKL) and decreased apoptotic markers (cleaved caspase-3 and cleaved caspase-8) were observed when HIF1α was knocked down in MC38 cells (online supplemental figure 5N). As a consequence, MC38 cells showed increased necrosis and less apoptosis after the knockdown of HIF1α (online supplemental figure 5O). Collectively, those data showed that HIF1α is a negative regulator of necroptosis in IECs.

HIF1α transcriptionally represses RIPK3

To elucidate how HIF1α inhibits necroptosis, small intestine organoids from *Hif1a*$^{\Delta IEC}$ and littermate control mice were exposed to hypoxic conditions. While WT organoids survived, *Hif1a*$^{\Delta IEC}$ organoids showed a deteriorated morphology (figure 5A and B). Immunofluorescence staining and qRT-PCR analyses showed increased mRNA levels of necroptotic genes *Ripk1*, *Ripk3* and *Mlkl*, as well as their phosphorylated protein forms, but reduced expression of *caspase-3* and *caspase-8* mRNA

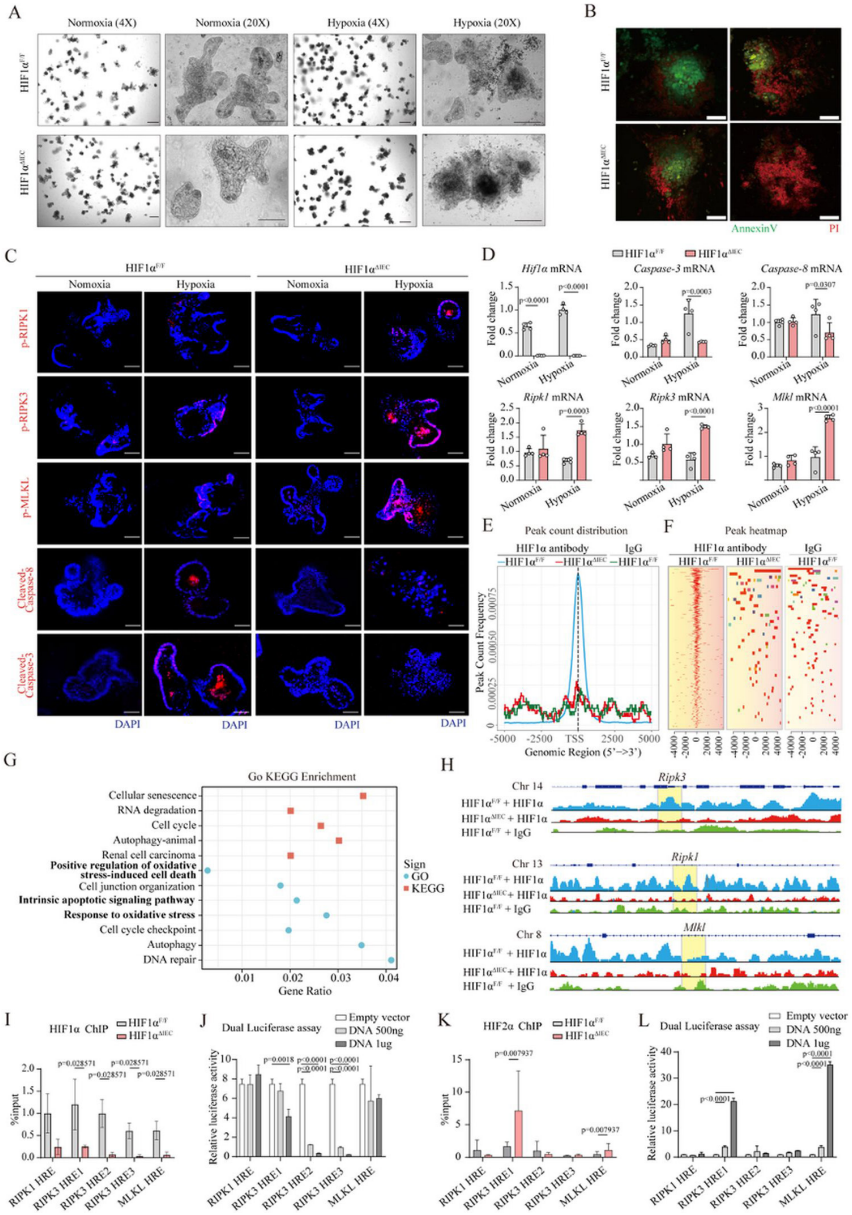

Figure 5 HIF1α transcriptionally represses RIPK3. (A) Representative brightfield overview and IF for (B) Annexin V and propidium iodide and (C) cleaved caspase-3 and caspase-8, p-RIPK1, p-RIPK3 and p-MLKL of intestinal organoids generated from HIF1α$^{\Delta IEC}$ C57BL/6 mice and littermate controls before and after exposure to 1% oxygen for 8 hours; scale bar 50 µm. (D) Quantitative real-time PCR analysis of *Hif1α*, *Caspase-3*, *Caspase-8*, *Ripk1*, *Ripk3* and *Mlkl* mRNA expression in intestinal organoids generated from HIF1α$^{\Delta IEC}$ C57BL/6 mice and littermate controls under normoxia and hypoxia (n=4). (E) ChIP DNA-sequencing peak count distribution and (F) heatmap of IECs from the ileum of HIF1α$^{\Delta IEC}$ C57BL/6 mice and littermate controls at day 36 pfi. (G) Dot plot of GO and KEGG pathway enrichment analysis comparing ChIP-Seq DEGs of HIF1α$^{\Delta IEC}$ C57BL/6 mice and littermate controls at day 36 pfi. () (H) Region of the promoter from +5000 bp to −5000 bp around the transcription start site of RefSeq genes. Genomic visualisation of HIF1α enrichment peak at the promoter regions of *Ripk1*, *Ripk3* and *Mlkl*. (I) ChIP-qPCR analysis of HIF1α enrichment to the predicted HRE regions within the *Ripk1*, *Ripk3* and *Mlkl* promoters from ileum IECs of HIF1α$^{\Delta IEC}$ C57BL/6 mice and littermate controls at day 36 pfi. Recruitment is expressed as a percentage of input DNA (n=3). (J) Luciferase reporter gene assay for *Ripk1*, *Ripk3* and *Mlkl* promoter activity in MC38 cells 48 hours after the transfection with different concentrations of HIF1αTM plasmid, Renilla plasmid and pGL4.23+*Ripk1*/*Ripk3*/*Mlkl* HREs plasmids (n=3–5). (K) ChIP-qPCR analysis of HIF2α enrichment to the predicted HRE regions within the *Ripk1*, *Ripk3* and *Mlkl* promoters from ileal IECs of HIF1α$^{\Delta IEC}$ mice and littermate controls at day 36 pfi. Recruitment is expressed as a percentage of input DNA (n=3). (L) Luciferase reporter gene assay for *Ripk1*, *Ripk3* and *Mlkl* promoter activity in shRNA HIF1α-knockdown MC38 cells 48 hours after the transfection with different concentrations of HIF2αTM plasmid, Renilla plasmid and pGL4.23+*Ripk1*/*Ripk3*/*Mlkl* HRE plasmids (n=3–5). Data are representative of three independent experiments. Data are shown as mean±SD. Statistical significance was determined by one-way ANOVA followed by (D) Tukey's test, multiple Mann-Whitney U tests followed by the corrected method of Benjamini and Yekutieli (I and K) and two-way ANOVA followed by Tukey's test (I and K). CIA, collagen-induced arthritis; ChIP, chromatin immunoprecipitation; DAPI, 4′,6-diamidino-2-phenylindole; DEGs, differentially expressed genes; EM, electron microscopy; FISH, fluorescence in situ hybridisation; GO, Gene Ontology; HIF, hypoxia-inducible factor; IEC, intestinal epithelial cells; IF, immunofluorescence; IL, interleukin; IFN-γ, interferon-gamma; KEGG, Kyoto Encyclopedia of Genes and Genomes; pfi, post-first immunisation; PAS, periodic acid Schiff; PP, Peyer's patches; PHD, prolyl-hydroxylase domain; µCT, micro-CT; MPO, myeloperoxidase; RA, rheumatoid arthritis; TRAP, tartrate-resistant acid phosphatase; TUNEL, terminal deoxynucleotidyl transferase dUTP nick end labelling.

or cleaved caspase-3 and caspase-8 proteins in *Hif1a*$^{\Delta IEC}$ organoids (figure 5C and D). To illustrate the function of HIF1α at the transcriptional level, we performed HIF1α ChIP-seq analysis on IECs from CIA WT and *Hif1a*$^{\Delta IEC}$ mice. HIF1α-regulated genes were defined after ChIP-seq data annotation (figure 5E) and comparison (figure 5F). GO and KEGG enrichment analyses showed that direct HIF1α target genes were associated with epithelial cell death and proliferation (figure 5G). Genomic data were visualised for *Ripk1*, *Ripk3* and *Mlkl* (figure 5H). Strong binding activity of HIF1α was observed at the *Ripk1*, *Ripk3* and *Mlkl* transcription start sites. *Ripk1*, *Ripk3 and Mlkl* HREs binding activities within 5000 bp upstream of the promoter region were then confirmed by HIF1α ChIP-qPCR (figure 5I). Each of the validated HRE fragments was cloned into a luciferase reporter plasmid for subsequent functional analyses in MC38 cells. Luciferase activity displayed a dose-dependent decrease for HRE2 and HRE3 from the *Ripk3* promoter (figure 5J). To explore possible regulatory functions of HIF2α in the absence of HIF1α, we performed HIF2α ChIP-qPCR and luciferase reporter assays on IECs from the ileum of WT and *Hif1a*$^{\Delta IEC}$ mice in steady state. We found that HIF2α binds as an enhancer on HRE1 of *Ripk3* and on *Mlkl* HREs in the absence of HIF1α (figure 5K and L). Taking together, increased necroptosis of IECs upon HIF1α deletion is likely due to its transcriptional function on the *Ripk3* promoter.

RIPK3 inhibition suppresses HIF1α$^{\Delta IEC}$-associated gut epithelial necroptosis and arthritis

To further characterise RIPK3-mediated necroptosis, we performed immunohistochemical staining of ileal biopsies from patients with new-onset RA. RIPK1, RIPK3 and MLKL were specifically expressed in IECs. MLKL expression was significantly elevated in patients with RA (online supplemental figure 6A–C). To determine the importance of RIPK3 in epithelial cell death induced by HIF1α deletion, we took advantage of intestinal organoids from the ileum of *Ripk3*$^{-/-}$ and littermate control mice exposed to hypoxic conditions. Interestingly, *Ripk3*$^{-/-}$ intestinal organoids exhibited higher survival rates (figure 6A and B), correlating with decreased mRNA expression of necroptosis-related genes such as *Mlkl*, *Hmgb-1* and *Tnfrsf1a* and increased *Caspase-3* mRNA expression in *Ripk3*$^{-/-}$ compared with WT cells exposed to hypoxia (figure 6C). To investigate the role of RIPK3-mediated necroptosis, we induced CIA in *Ripk3*$^{-/-}$, *Mlkl*$^{-/-}$ and *Ripk3*$^{-/-}$*Mlkl*$^{-/-}$ mice. The results showed that these genetically modified mice had lower clinical scores and a reduced incidence of arthritis compared with their respective littermate controls (online supplemental figure 7A and D).

To clarify the pathways of IEC death under hypoxic conditions, we exposed WT intestinal organoids to different hypoxic stimuli and treated them with inhibitors that target either the apoptosis or necroptosis pathways. The study found that the pan-caspase inhibitor, Z-VAD-FMK, effectively improved organoid viability when exposed to moderate hypoxia (5% oxygen), as shown in online supplemental figure 7C and D. In contrast, WT organoids exposed to severe hypoxia (1% oxygen) showed improved survival rates with the use of necroptosis inhibitors, such as necrostain-1 and GSK'872 (online supplemental figure 7E).

To investigate the involvement of HIF1α-associated necroptosis in a hypoxic environment, *Hif1α*$^{\Delta IEC}$ organoids were exposed to 1% oxygen for 8 hours. The results showed that *Hif1α*$^{\Delta IEC}$ organoids adapted better to hypoxia, especially when treated with RIPK3 inhibitors, as opposed to pan-caspase or RIPK1 inhibitors (figure 6D–E and online supplemental figure 7F). Molecularly, in WT organoids, expression of both apoptotic (*Caspase-3* and *Caspase-8*) and necroptotic (*Ripk1*, *Ripk3*, *Mlkl* and *Hmgb-1*) markers was inhibited by GSK'872 treatment after 8 hours of 1% oxygen treatment, whereas only the expression of necroptotic genes was inhibited in *Hif1a*$^{\Delta IEC}$ organoids (figure 6F). Treatment of CIA mice with GSK'872 from day 14 to day 36 pfi led to the inhibition of arthritis development in WT and *Hif1a*$^{\Delta IEC}$ mice (figure 7A). Arthritis incidence was also decreased upon RIPK3 inhibition (figure 7B). Th1 and Th17 cells in PPs and MLN were decreased in *Hif1a*$^{\Delta IEC}$ CIA mice (figure 7C and D), while no significant difference was observed in the spleen (figure 7E). IL-17A and IFN-γ serum levels were also lower upon RIPK3 inhibition *in Hif1a*$^{\Delta IEC}$ CIA mice (figure 7F). Rescue of intestinal inflammation, bacterial translocation and IEC death was observed in *Hif1a*$^{\Delta IEC}$ CIA mice after RIPK3 inhibition (figure 7G–J, online supplemental figure 8A–D). Moreover, expression of necroptotic (*Ripk3*, *Mlkl*, *Hmgb-1* and *Tnfrsf1a*) and inflammatory (*Il-1β*, *Il-6*, *Tnf*, *Ifn-γ* and *Il-17*) genes tended to decrease in IECs from WT and *Hif1a*$^{\Delta IEC}$ CIA mice without triggering additional cleaved-caspase-3 activation, after RIPK3 inhibition when compared with their respective vehicle controls (figure 7K–L, online supplemental figure 8E–F). Taking together, our data demonstrated that inhibition of RIPK3 alleviated IEC necroptosis and the development of arthritis. online supplemental figure 9online supplement figure 9

DISCUSSION

Here, we show that the control of necroptosis in IEC is an important regulatory mechanism in the development of arthritis. Both experimental murine and human arthritis are characterised by increased necroptosis of IEC at disease onset. This process is inhibited by HIF1α because HIF1α inhibits expression of the key necroptotic factor RIPK3 and thereby blocks IEC death, maintains barrier function and inhibits arthritis. Both pharmacological stabilisation of HIF-1α and inhibition of RIPK3 effectively reduced arthritis, indicating that IEC death is a critical factor for arthritis onset.

While the role of the intestinal barrier on arthritis has been studied previously and tight junction proteins, such as claudins and occludin, have been reported to play in intestinal barrier function and the development of arthritis,[6 26] it has remained unclear whether and how IEC death influences arthritis. Studies on the role of IEC death have so far been limited in studying its role in experimental models of colitis and in patients with Crohn's disease.[10 27] By integrating data from previous research, our investigation shows that the death of IEC occurs after intestinal barrier dysfunction, microbial dysbiosis and increased expression of zonulin.[6] This establishes a sequential progression of events, making a significant contribution to the existing body of knowledge.

Necroptosis is a programmed cell death[28] that can trigger proinflammatory effects by releasing damage-associated molecular patterns.[29] Our analysis of cell death in the intestinal epithelium during the onset of arthritis shows activation of necroptotic molecules such as RIPK3 and MLKL. Necroptosis of the IEC disrupts the intestinal barrier, promotes intestinal inflammation and exacerbates arthritis. The role of necroptosis in intestinal inflammation is also highlighted by the effects of the RIPK3 inhibitor, GSK'872, in inhibiting dextran sulphate sodium-induced colitis.[30 31] Here, we show that this RIPK3-induced necroptosis has effects that go beyond intestinal inflammation, as necroptosis of the IEC appears to shape an intestinal environment that promotes arthritis.

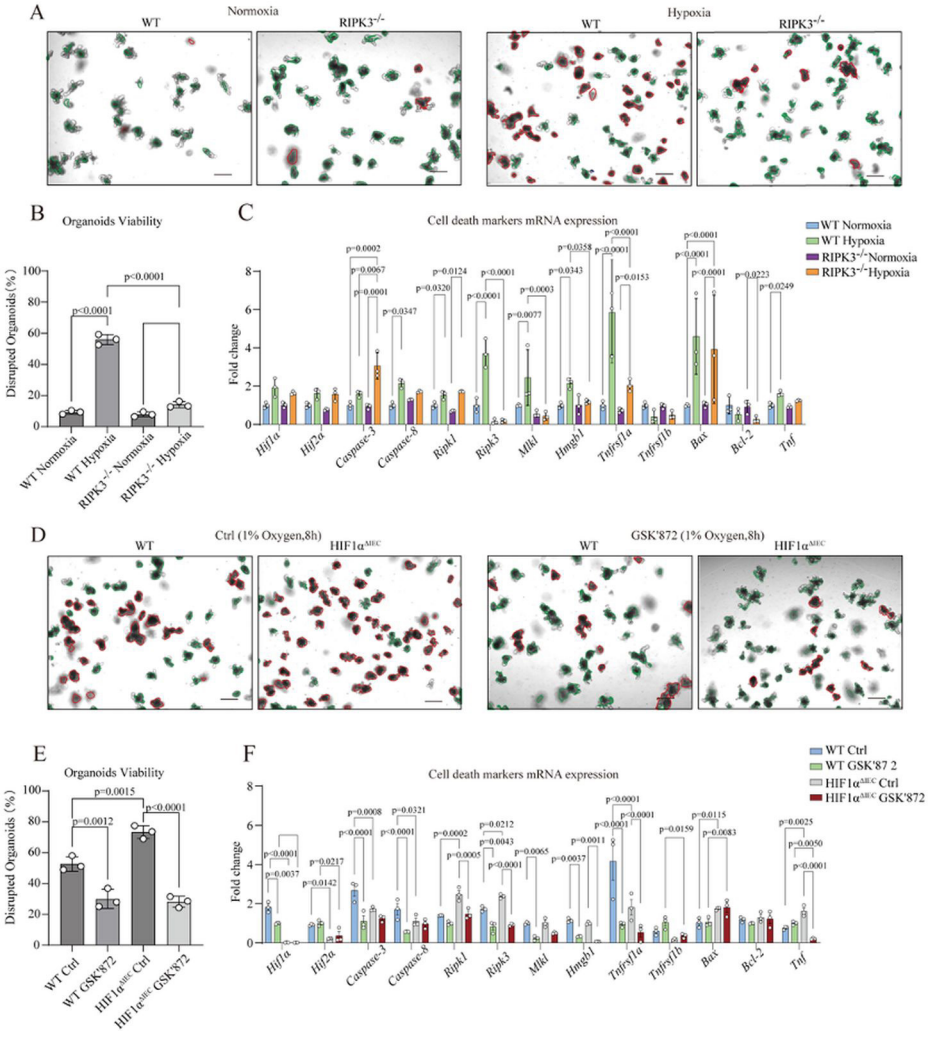

Figure 6 RIPK3 inhibition rescues HIF1α deletion-associated intestinal epithelial cell necroptosis in vitro. (A) Representative images, (B) quantification of viability and (C) quantitative real-time PCR analysis of *Hif1α*, *Hif2α*, *Caspase3*, *Caspase8*, *Ripk1*, *Ripk3*, *Mlkl*, *Hmgb1*, *Tnfrsf1a*, *Tnfrsf1b*, *Bax*, *Bcl-2* and *Tnf* mRNA expression in intestinal organoids generated from RIPK3$^{-/-}$ C57BL/6 mice and littermate controls before and after exposure to 1% oxygen for 8 hours; scale bar 50 µm. (D) Representative images, (E) quantification of viability and (F) quantitative real-time PCR analysis regarding *Hif1α*, *Hif2α*, *Caspase3*, *Caspase8*, *Ripk1*, *Ripk3*, *Mlkl*, *Hmgb1*, *Tnfrsf1a*, *Tnfrsf1b*, *Bax*, *Bcl-2* and *Tnf* mRNA expression of intestinal organoids generated from HIF1α$^{\Delta IEC}$ C57BL/6 mice and littermate controls after exposure to 1% oxygen for 8 hours, without or with treatment with 5 µm RIPK3 inhibitor GSK'872. Data are shown as mean±SD. Statistical significance was determined by (B and E) one-way ANOVA followed by Tukey's test and (C and F) two-way ANOVA followed by Tukey's test. ANOVA, analysis of variance; HIF, hypoxia-inducible factor; RIPK3, receptor-interacting protein kinase-3; WT, wild-type.

The microenvironment is an essential component in the maintenance of the IECs. Inflammation is leading to a sustained hypoxic environment.[13 14 32] Our previous and current data indicated an induction of the HIFs, HIF1α and HIF2α, in the intestinal epithelium during experimental arthritis and in patients with RA.[7] These data show that stabilisation of HIF1α represses necroptosis of IECs and thereby minimises inflammatory damage. While both HIF2α and HIF1α mediate the cellular response to hypoxia, they have fundamentally different transcriptional functions in the intestine. Expression of HIF2α by IECs disrupts intestinal barrier functions by enhancing the transcription of claudin-15, which facilitates intestinal permeability and exacerbates intestinal inflammation and arthritis.[7] HIF1α has opposing effects as it protects IECs and barrier function.[33 34]. Under normoxic conditions, the PHD/pVHL axis prohibits RIPK1-induced cytotoxicity through the PHD-mediated hydroxylation of RIPK1.[35] Experiments have evidenced that insufficient hydroxylation of RIPK1 due to severe hypoxia or PHD inhibition can directly promote cell death either through RIPK3/MLKL activation or apoptosis, depending on the context, and independently of HIF1α induction.[35] Remarkably, we observed a significant increase in HIF1α protein levels in the ileum of CIA mice at day 20 pfi, despite no significant change in mRNA expression levels. This finding highlights the complex regulation of HIF1α proteins, which is governed by both transcriptional and post-translational processes. Fostering HIF1α activity, for example, through targeting the HIF-PHD pathway, is therefore a potentially interesting approach to mitigate or stop the onset of arthritis.[17 36 37] Roxadustat, a small molecular HIF-PHD inhibitor that enhances HIF1α activity, has been approved for the treatment of anaemia and chronic kidney disease in humans. Notably, the assessment report of roxadustat provided by the European Medicines Agency (EMA/CHMP/393136/2021) shows its preferential distribution in the gastrointestinal tract subsequent to oral administration in vivo. Hence, it is possible that the effects of roxadustat on the gut

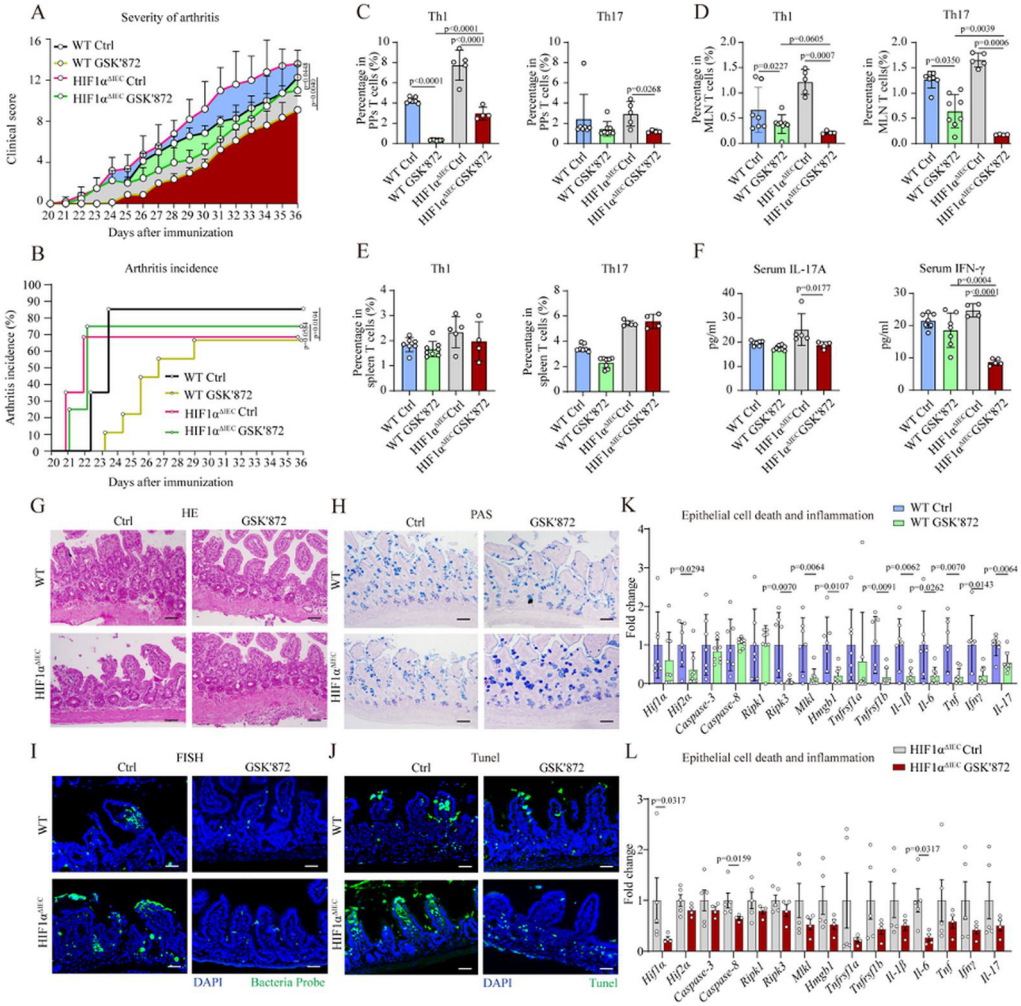

Figure 7 RIPK3 inhibition rescues HIF1α deletion-associated intestinal epithelial cell necroptosis and arthritis in vivo. (A) Clinical score and (B) arthritis incidence in HIF1α$^{\Delta IEC}$ C57BL/6 mice and littermate controls subjected to CIA and treated with or without RIPK3 inhibitor GSK'872 (n=7, 8, 5 and 4, respectively). Fluorescence-activated cell sorting quantification of Th17 and Th1 cells in (C) PPs, (D) mesenteric lymph nodes and (E) spleen from HIF1α$^{\Delta IEC}$ C57BL/6 mice and littermate controls subjected to CIA and treated with or without RIPK3 inhibitor GSK'872; day 36 pfi; n=7, 8, 5 and 4, respectively. Data are representative of three independent experiments. Symbols represent individual mice. (F) Serum IL-17A and IFN-γ levels measured by ELISA from HIF1α$^{\Delta IEC}$ C57BL/6 mice and littermate controls subjected to CIA and treated with or without RIPK3 inhibitor GSK'872 (n=7, 8, 5 and 4, respectively; day 36 pfi). () Representative images of (G) H&E, (H) PAS, (I) FISH and (J) TUNEL staining in the ileum from C57BL/6 CIA mice gavaged with GSK'872 or vehicle control at day 36 pfi. (K–L) Quantitative real-time PCR analysis of *Hif1α*, *Hif2α*, *Caspase3*, *Caspase8*, *Ripk1*, *Ripk3*, *Mlkl*, *Hmgb1*, *Tnfrsf1a*, *Tnfrsf1b*, *Il-β*, *Il-6*, *Tnf*, *Ifnγ* and *Il-17* mRNA expression in IECs from HIF1α$^{\Delta IEC}$ C57BL/6 mice and respective littermate controls with or without GSK'872 treatment (day 36 pfi; n=7, 8, 5 and 4, respectively). Data are shown as mean±SD. Statistical significance was determined by Kaplan-Meier analysis with (A) log-rank test, (B) χ^2 test, (C–F) one-way analysis of variance followed by Tukey's test or Kruskal-Wallis H test followed by Dunn's test or (K and L) multiple Mann-Whitney U tests followed by corrected method of Benjamini and Yekutieli. CIA, collagen-induced arthritis; DAPI, 4′,6-diamidino-2-phenylindole; FISH, fluorescence in situ hybridisation; HIF, hypoxia-inducible factor; IEC, intestinal epithelial cells; IL, interleukin; IFN-γ, interferon-gamma; PAS, periodic acid Schiff; pfi, post-first immunisation; PAS, periodic acid Schiff; PP, Peyer's patches; RIPK3, receptor-interacting protein kinase-3; TUNEL, terminal deoxynucleotidyl transferase dUTP nick end labelling; WT, wild-type.

reported in this paper may also be seen in humans. By inhibiting intestinal necroptosis, roxadustat may potentially alleviate human arthritis, thereby offering an additional promising angle to modulate arthritis by influencing disease-promoting factors outside the joints. In addition, roxadustat may exert beneficial effects on anaemia, which is common in individuals with RA.

The results from this study are nonetheless limited to expression data in mice, humans and experimental models, while no roxadustat treatment has been done in patients with RA. Hence, it is not clear whether roxadustat would ameliorate RA. However, as oral roxadustat is distributed in the gut in humans, it is likely that it exerts antinecroptotic effects in human IECs, providing the basis for a potential effect in human arthritis. Another limitation is that some additional roles of proapoptotic pathways can not be completely ruled out. The intricate mechanisms governing the crosstalk between RIPK3 and other cell death pathways, such as apoptosis, are multifaceted.[38 39] It is important to note that RIPK3 inhibitors have been primarily developed and used to inhibit necroptosis and regulate the inflammatory responses associated with RIPK3 activation.[40 41] However, while we did not find any cleaved-caspase-3 activation, it cannot be conclusively ruled out that necroptosis is the sole cause of cell death in intestinal epithelial cells during arthritis.

Taken together, these data show that IEC homeostasis influences arthritis. RIPK3-induced necroptosis of IEC enhanced arthritis, suggesting the existence of an intestinal pathway

enhancing the development of arthritis. On the other hand, HIF stabilisation by roxadustat and inhibition of RIPK3 provide new possibilities to inhibit intestinal epithelial necroptosis and therefore mitigate arthritis.

Author affiliations
[1]Department of Internal Medicine 3, Rheumatology and Immunology, Friedrich-Alexander University (FAU) Erlangen-Nürnberg and Universitätsklinikum Erlangen, Erlangen, Germany
[2]Deutsches Zentrum Immuntherapie, Friedrich-Alexander University (FAU) Erlangen-Nürnberg and Universitätsklinikum Erlangen, Erlangen, Germany
[3]Department of Internal Medicine 1, Friedrich-Alexander University (FAU) Erlangen-Nürnberg and Universitätsklinikum Erlangen, Erlangen, Bayern, Germany
[4]Department of Opthalmology, Friedrich-Alexander University (FAU) Erlangen-Nürnberg and Universitätsklinikum Erlangen, Erlangen, Germany
[5]Precision Medicine, Università degli Studi della Campania Luigi Vanvitelli, Napoli, Campania, Italy
[6]Microbiology Institute, Friedrich-Alexander University (FAU) Erlangen-Nürnberg and Universitätsklinikum Erlangen, Erlangen, Germany

X Daniele Mauro @dranielmar

Acknowledgements Thanks to the excellent technical assistance of Christine Zech, Franceska Jelas, Daniela Weidner, Dr Wolfgang Baum, Katharina Falk, Barbara Happich, Hilal Durmarz and Hedwig Symowski.

Contributors PL and AB designed the study and wrote the manuscript. PL and NL performed the in vitro experiments. PL, JW, IS, YJ, CG and FZ performed the in vivo experiments. DS contributed to manuscript preparation. DM and FC generated the human experiments. WZ analyzed the RNA-seq and ChIP-seq data. GS and AB supervised the study, wrote the manuscript and are responsible for the overall content.

Funding This work was supported by the Deutsche Forschungsgemeinschaft (FOR 2886-TP02, CRC 1181 project A01, SPP2084 µBone, and TRR369-project A02 and B05, OICE-STED: 263718168, OICE-Leica Stellaris: 441730715, OICE-Leica Thunder: 450993414), the ELAN-Programme (P044) of the Universitätsklinikum Erlangen, the Interdisciplinary Centre for Clinical Research (grant F1-04) in Erlangen, the European Research Council (ERC) consolidator grant ODE and synergy grant 4D Nanoscope and the Bundesministerium für Bildung und Forschung (project MASCARA) and the ERC the IMI funded project RTCure.Leica Stellaris: 441730715

Competing interests None declared.

Patient and public involvement Patients and/or the public were not involved in the design, or conduct, or reporting, or dissemination plans of this research.

Patient consent for publication Not applicable.

Ethics approval This study involves human participants and was approved by Rheumatology Section, Department of Health Promotion, Mother and Child Care, Internal Medicine and Medical Specialties, University Hospital P. Giaccone, Palermo, Italy. Participants gave informed consent to participate in the study before taking part.

Provenance and peer review Not commissioned; externally peer reviewed.

Data availability statement All data relevant to the study are included in the article or uploaded as supplementary information. The RNA-seq data used in this paper have been uploaded at GEO database (GSE175907, GSE176266 and GSE225597). The ChIP-Seq data used in this paper have been uploaded at GEO database (GSE225594).

ORCID iDs
Daniele Mauro http://orcid.org/0000-0002-9022-8863
Francesco Ciccia http://orcid.org/0000-0002-9352-1264
Georg Schett http://orcid.org/0000-0001-8740-9615
Aline Bozec http://orcid.org/0000-0001-8174-2118

REFERENCES

1 Chow J, Tang H, Mazmanian SK. Pathobionts of the gastrointestinal Microbiota and inflammatory disease. *Curr Opin Immunol* 2011;23:473–80.
2 Zaiss MM, Joyce Wu H-J, Mauro D, *et al*. The gut–joint axis in rheumatoid arthritis. *Nat Rev Rheumatol* 2021;17:224–37.
3 Maeda Y, Kurakawa T, Umemoto E, *et al*. Dysbiosis contributes to arthritis development via activation of Autoreactive T cells in the intestine. *Arthritis & Rheumatology* 2016;68:2646–61. 10.1002/art.39783 Available: https://acrjournals.onlinelibrary.wiley.com/toc/23265205/68/11
4 Alpizar-Rodriguez D, Lesker TR, Gronow A, *et al*. Prevotella Copri in individuals at risk for rheumatoid arthritis. *Ann Rheum Dis* 2019;78:590–3.
5 Fasano A. Zonulin and its regulation of intestinal barrier function: the biological door to inflammation, Autoimmunity, and cancer. *Physiological Reviews* 2011;91:151–75.
6 Tajik N, Frech M, Schulz O, *et al*. Targeting Zonulin and intestinal epithelial barrier function to prevent onset of arthritis. *Nat Commun* 2020;11.
7 Wen J, Lyu P, Stolzer I, *et al*. Epithelial Hif2A expression induces intestinal barrier dysfunction and exacerbation of arthritis. *Ann Rheum Dis* 2022;81:1119–30.
8 Blander JM. Death in the intestinal epithelium—basic biology and implications for inflammatory bowel disease. *FEBS J* 2016;283:2720–30.
9 Werts AD, Fulton WB, Ladd MR, *et al*. A novel role for Necroptosis in the pathogenesis of necrotizing Enterocolitis. *Cell Mol Gastroenterol Hepatol* 2020;9:403–23.
10 Günther C, Martini E, Wittkopf N, *et al*. Caspase-8 regulates TNF-A-induced epithelial Necroptosis and terminal Ileitis. *Nature* 2011;477:335–9.
11 Landers CJ, Cohavy O, Misra R, *et al*. Selected loss of tolerance evidenced by Crohn's disease–associated immune responses to auto-and microbial antigens. *Gastroenterology* 2002;123:689–99.
12 Fouser LA, Wright JF, Dunussi-Joannopoulos K, *et al*. Th17 Cytokines and their emerging roles in inflammation and Autoimmunity. *Immunol Rev* 2008;226:87–102.
13 Taylor CT, Colgan SP. Hypoxia and gastrointestinal disease. *J Mol Med (Berl)* 2007;85:1295–300.
14 Luo H, Guo P, Zhou Q. Role of Tlr4/NF-KB in damage to intestinal mucosa barrier function and bacterial translocation in rats exposed to hypoxia. *PLOS ONE* 2012;7:e46291.
15 Downes NL, Laham-Karam N, Kaikkonen MU, *et al*. Differential but complementary Hif1A and Hif2A transcriptional regulation. *Mol Ther* 2018;26:1735–45.
16 Karhausen J, Furuta GT, Tomaszewski JE, *et al*. Epithelial hypoxia-inducible Factor-1 is protective in murine experimental colitis. *J Clin Invest* 2004;114:1098–106.
17 Kim Y-I, Yi E-J, Kim Y-D, *et al*. Local stabilization of hypoxia-inducible Factor-1A controls intestinal inflammation via enhanced gut barrier function and immune regulation. *Front Immunol* 2020;11.
18 Taylor CT, Doherty G, Fallon PG, *et al*. Hypoxia-dependent regulation of inflammatory pathways in immune cells. *J Clin Invest* 2016;126:3716–24.
19 Ryan HE, Poloni M, McNulty W, *et al*. Hypoxia-inducible Factor-1Alpha is a positive factor in solid tumor growth. *Cancer Res* 2000;60:4010–5.
20 Madison BB, Dunbar L, Qiao XT, *et al*. Cis elements of the Villin gene control expression in restricted domains of the vertical (crypt) and horizontal (duodenum, Cecum) axes of the intestine. *J Biol Chem* 2002;277:33275–83.
21 Newton K, Sun X, Dixit V. Kinase Rip3 is Dispensable for normal NF-Kbs, signaling by the B-cell and T-cell receptors, tumor necrosis factor receptor 1, and toll-like receptors 2 and 4. *Mol Cell Biol* 2004;24:1464–9.
22 Murphy JM, Czabotar PE, Hildebrand JM, *et al*. The Pseudokinase MLKL mediates Necroptosis via a molecular switch mechanism. *Immunity* 2013;39:443–53.
23 Sato T, Vries RG, Snippert HJ, *et al*. Single Lgr5 stem cells build crypt-Villus structures in vitro without a Mesenchymal niche. *Nature* 2009;459:262–5.
24 Erben U, Loddenkemper C, Doerfel K, *et al*. A guide to Histomorphological evaluation of intestinal inflammation in Mouse models. *Int J Clin Exp Pathol* 2014;7:4557–76.
25 O'Rourke KP, Dow LE, Lowe SW. Immunofluorescent staining of Mouse intestinal stem cells. *Bio Protoc* 2016;6:e1732.
26 Saeedi BJ, Kao DJ, Kitzenberg DA, *et al*. HIF-dependent regulation of Claudin-1 is central to intestinal epithelial tight junction integrity. *Mol Biol Cell* 2015;26:2252–62.
27 Duan C, Xu X, Lu X, *et al*. Rip3 knockdown inhibits Necroptosis of human intestinal epithelial cells via Tlr4/Myd88/NF-KB signaling and ameliorates murine colitis. *BMC Gastroenterol* 2022;22.
28 O'Donnell MA, Perez-Jimenez E, Oberst A, *et al*. Caspase 8 inhibits programmed necrosis by processing CYLD. *Nat Cell Biol* 2011;13:1437–42.
29 Dhuriya YK, Sharma D. Necroptosis: a regulated inflammatory mode of cell death. *J Neuroinflammation* 2018;15.
30 Zhou M, He J, Shi Y, *et al*. Abin3 negatively regulates Necroptosis-induced intestinal inflammation through recruiting A20 and restricting the Ubiquitination of Ripk3 in inflammatory bowel disease. *Journal of Crohn's and Colitis* 2021;15:99–114.
31 Lee SH, Kwon JY, Moon J, *et al*. Inhibition of Ripk3 pathway attenuates intestinal inflammation and cell death of inflammatory bowel disease and suppresses Necroptosis in peripheral mononuclear cells of ulcerative colitis patients. *Immune Netw* 2020;20.

32 Taylor CT. Hypoxia in the gut. *Cell Mol Gastroenterol Hepatol* 2018;5:61–2.
33 Dowdell AS, Cartwright IM, Goldberg MS, *et al*. The HIF target Atg9A is essential for epithelial barrier function and tight junction Biogenesis. *Mol Biol Cell* 2020;31:2249–58.
34 Daskalaki I, Gkikas I, Tavernarakis N. Hypoxia and selective Autophagy in cancer development and therapy. *Front Cell Dev Biol* 2018;6.
35 Zhang T, Xu D, Liu J, *et al*. Prolonged hypoxia Alleviates Prolyl hydroxylation-mediated suppression of Ripk1 to promote Necroptosis and inflammation. *Nat Cell Biol* 2023;25:950–62.
36 Bakshi HA, Mishra V, Satija S, *et al*. Dynamics of Prolyl Hydroxylases levels during disease progression in experimental colitis. *Inflammation* 2019;42:2032–6.
37 Cummins EP, Seeballuck F, Keely SJ, *et al*. The hydroxylase inhibitor Dimethyloxalylglycine is protective in a murine model of colitis. *Gastroenterology* 2008;134:156–65.
38 Mandal P, Berger SB, Pillay S, *et al*. Rip3 induces apoptosis independent of Pronecrotic kinase activity. *Mol Cell* 2014;56:481–95.
39 Lawlor KE, Khan N, Mildenhall A, *et al*. Ripk3 promotes cell death and Nlrp3 Inflammasome activation in the absence of MLKL. *Nat Commun* 2015;6.
40 Gong Y, Fan Z, Luo G, *et al*. The role of Necroptosis in cancer biology and therapy. *Mol Cancer* 2019;18.
41 Liu Y, Liu T, Lei T, *et al*. Rip1/Rip3-regulated Necroptosis as a target for Multifaceted disease therapy. *Int J Mol Med* 2019;44:771–86.